IOP Publishing New J. Phys. 25 (2023) 093034 https://doi.org/10.1088/1367-2630/acf151

New Journal of Physics
The open access journal at the forefront of physics

Deutsche Physikalische Gesellschaft DPG
IOP Institute of Physics

Published in partnership with: Deutsche Physikalische Gesellschaft and the Institute of Physics

OPEN ACCESS

RECEIVED
21 January 2023

REVISED
28 July 2023

ACCEPTED FOR PUBLICATION
17 August 2023

PUBLISHED
15 September 2023

PAPER

Unpredictability and entanglement in open quantum systems

Javad Kazemi* and Hendrik Weimer*

Institut für Theoretische Physik, Leibniz Universität Hannover, Appelstraße 2, 30167 Hannover, Germany
* Authors to whom any correspondence should be addressed.

E-mail: javad.kazemi@itp.uni-hannover.de and hweimer@itp.uni-hannover.de

Keywords: elementary cellular automata, computational unpredictability, variational quantum simulation

Abstract

We investigate dynamical many-body systems capable of universal computation, which leads to their properties being unpredictable unless the dynamics is simulated from the beginning to the end. Unpredictable behavior can be quantitatively assessed in terms of a data compression of the states occurring during the time evolution, which is closely related to their Kolmogorov complexity. We analyze a master equation embedding of classical cellular automata and demonstrate the existence of a phase transition between predictable and unpredictable behavior as a function of the random error introduced by the probabilistic character of the embedding. We then turn to have this dynamics competing with a second process inducing quantum fluctuations and dissipatively driving the system to a highly entangled steady state. Strikingly, for intermediate strength of the quantum fluctuations, we find that both unpredictability and quantum entanglement can coexist even in the long time limit. Finally, we show that the required many-body interactions for the cellular automaton embedding can be efficiently realized within a variational quantum simulator platform based on ultracold Rydberg atoms with high fidelity.

1. Introduction

The discovery of problems that are fundamentally undecidable is one of the most striking results in the history of mathematics [1, 2]. For physical systems, this means that certain problems such as the existence of a spectral gap in a many-body system can be undecidable as well [3–5]. Likewise, the long-term dynamics of a physical system can be *unpredictable* in the sense that the only way to compute observables is to simulate the system from the beginning to the end [6]. Here, we show that driven-dissipative quantum systems provide an ideal platform to study such fascinating systems and to explore the hitherto largely unknown relation of this unpredictably with entanglement that is absent in classical dynamical systems. Strikingly, while we find that the statistical aspects of entangled states inherently drive the system towards chaotic behavior, we find that under the right conditions, unpredictability and entanglement can coexist in the steady state.

The dynamical behavior of unpredictable systems is most readily analyzed in the framework of cellular automata (CA), as one can show rigorously that these systems are Turing-complete and hence unpredictable [7–10]. However, common quantum version of CA [11–15] rely on purely unitary dynamics and are therefore challenging to realize without having access to fault-tolerant quantum computers. For this reason, variants of quantum CA using open quantum many-body systems [16, 17] appear to be a much more promising route to investigate the interplay between unpredictability and inherently quantum properties of the dynamics like quantum superpositions and entanglement.

In this article, we provide an embedding of CA into a Lindblad master equation, which is commonly used within open quantum systems. To this end, we consider two coupled one-dimensional (1D) chains representing the state of the automaton at the time step t and $t+1$, respectively, see figure 1(a). Here, we focus on a class of elementary CA introduced by Wolfram [18], as this class contains Turing-complete automata and can be realized in the embedding using at most four-body interactions. The mapping of CAs onto master equation requires a periodic switching of the chains, with the exact CA dynamics being recovered in the limit of infinite cycle times. Interestingly, the imperfections to the perfect CA rules introduced by finite cycle times do not immediately destroy unpredictability, as shown using an

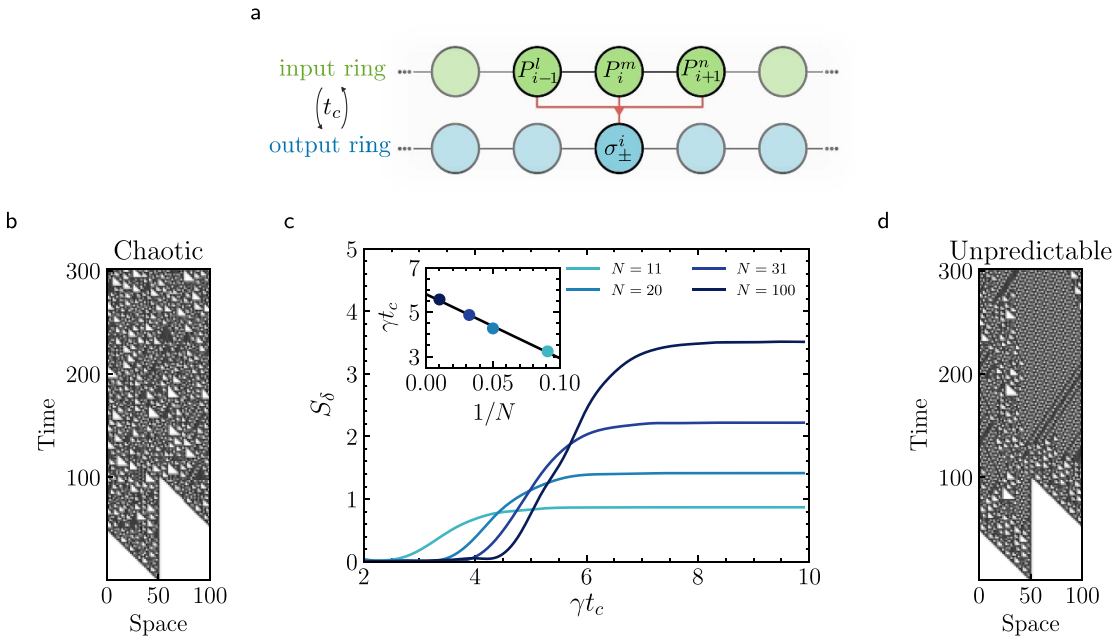

Figure 1. (a) Physical implementation of elementary CA on two rings of lattice sites, with the input and output ring switching after a cycle time t_c. (b) Typical trajectory of the rule 110 CA evolving from a single cell in the 1 state (black) for a short cycle time $t_c = 4/\gamma$, leading to Class III chaotic behavior. (c) Increasing the cycle time induces a transition to unpredictable behavior as shown by the slope S_δ of the characteristic compression exponent. Finite size scaling (inset) points to a value of $\gamma t_c = 5.80 \pm 0.08$ for the transition in the thermodynamic limit. (d) Typical trajectory in the unpredictable Class IV phase at a large cycle time $t_c = 10/\gamma$. At longer times, emergent glider structures propagating through the systems become clearly visible. Calculations were made at $n = 50$ and $t = 300$ to obtain convergence in S_δ. For each initial state, 100 Monte-Carlo samples were taken.

information-theoretical complexity measure based on data compression of the states during the dynamical evolution of the system [19]. We then introduce quantum fluctuations by adding a second set of terms to the master equation that drive the system to a highly-entangled Rokhsar–Kivelson state [20]. We explore the interplay between unpredictability and entanglement by modifying the relative rates of the two competing dynamics, finding an intermediate regime in which both entanglement and unpredictability coexist. Finally, we demonstrate the experimental feasibility of our approach by investigating a platform based on ultracold Rydberg atoms [21, 22]. To this end, we introduce an open system version of a variational quantum estimation algorithm [23–25] and show that the full dynamics including dissipative many-body interactions can be realized efficiently.

2. Complexity classes and unpredictability

The fundamental properties of the dynamical evolution of translation invariant dynamical systems like CAs can be broadly captured in four distinct classes [6, 26], referring to their generic behavior for almost all initial states. Class I refers to a fast evolution towards a steady state. Class I behavior is present in many driven-dissipative systems with detailed balance. Class II systems evolve towards periodic limit-cycle oscillations. A paradigmatic example of Class II is time crystals, systems that change their properties periodicity in time instead of space, for a review see [27]. Class III systems are chaotic, which can be captured in terms of a positive Lyapunov exponent [28] and fast relaxation of entropic measures to a constant value that is large. Lorenz systems exhibit Class III behavior that illustrates the challenges of long-term weather forecasting, see e.g. [29]. Finally, Class IV systems exhibit diverging correlation lengths, emerging structures that can be very complex, and other statistical features [30]. It is conjectured that Class IV systems are capable of universal computation and hence their behavior in the thermodynamic limit is fundamentally uncomputable [6]. It has also been discussed that Class IV systems are critical phases at the edge between regular periodic and chaotic behavior [30]. A well-known example of this class is Conway's game of life [31].

While chaotic (i.e. Class III) systems are sometimes also classified as unpredictable because of their sensitivity to changes in the initial condition, the notion of unpredictability we employ here is more strict, as statements about *some* long-time properties of chaotic systems are possible in terms of statistical averages, e.g. by coarse-graining the system under consideration [32]. Our notion of unpredictability is closely connected to the concept of *sophistication* in computer science [33], which can also be understood as capturing the complexity of systems at a coarse-grained level [34].

Table 1. Classification of dynamical behavior in translation invariant systems based on data compression measures. Class I and II can be distinguished from III and IV, as the asymptotic state S can be highly compressed for the first two classes, while the last two are essentially incompressible. The second classifier is the sensitivity of the compression length to changes in the initial state, captured in the slope S_δ of the characteristic compression exponent.

	Class I	Class II	Class III	Class IV
Dynamical behavior	Uniform	Periodic	Chaotic	Unpredictable
compressed length $\mathcal{C}_c(S)$	$\mathcal{C}_c(S) \ll S$		$\mathcal{C}_c(S) \approx S$	
Slope S_δ	Vanishing	Finite	Vanishing	Finite

The quantitative identification of Class IV behavior is extremely challenging, requiring the computation of observables that go beyond entropic measures or Lyapunov exponents geared to the analysis of Class III systems. For systems of discrete variables, one possibility is an information-theoretical analysis of the computational strings encoding the state of the system. For each string S, the algorithmic complexity is given by its Kolmogorov complexity $\mathcal{K}(S)$, which is defined as the length of the shortest program that can output S [35]. However, Kolmogorov complexity itself is an uncomputable quantity, preventing a direct practical application. Fortunately, it is possible to construct practically useful complexity measures by considering the compression length $\mathcal{C}(S) = \mathcal{C}_c(S) + \mathcal{C}_0$ where $\mathcal{C}_c(S)$ is the compressed length of S using a compression program of length $\mathcal{C}_0$, the latter being the same for all strings S. We would like to note that $\mathcal{C}_c(S)$ can be seen as an upper bound to the Kolmogorov complexity, i.e. $\mathcal{K}(S) \leqslant \mathcal{C}_c(S)$, but it is not necessarily a particular tight bound for all types of dynamics; for our purposes, it is more important that it is a measure that is not biased towards particular dynamical systems.

For the classification of dynamical systems, the Kolmogorov complexity (or the compression length) is not sufficient to capture unpredictability, as the (pseudo-)randomness inherent in chaotic systems will generically lead to large values of $\mathcal{K}(S)$ even for Class III systems. However, it is possible to differentiate Class III and Class IV by looking at the compression length for different initial states [19, 26], see table 1. For chaotic Class III systems, the Kolmogorov complexity does not depend on the particular initial state, i.e. differential measures of Kolmogorov complexity are vanishing. Importantly, this is not the case in Class IV systems, where the Kolmogorov complexity strongly depends on the initial state. This can be understood as the initial state encoding a program that is run using the universal computing capabilities of the Class IV system. Some programs can produce simple computing results exhibiting a low Kolmogorov complexity, while others can lead to arbitrary complex computations. This can be captured quantitatively in the form of a characteristic compression exponent [19], which is a generalization of the Lyapunov exponent to algorithmic complexity. It is given by

$$\delta_n(t) = \sum_{j=1}^{n-1} \frac{\left|\bar{\mathcal{C}}_c(S_j(t)) - \bar{\mathcal{C}}_c(S_{j+1}(t))\right|}{n-1}, \tag{1}$$

where $S_j(t)$ refers to the string representation of the entire evolution of the system up to the time t for the jth initial state and the sum runs over n initial states in total. Here we estimate $S_j(t)$ by Monte-Carlo sampling and afterwards we average the corresponding compressed lengths denoted by $\bar{\mathcal{C}}_c$. For systems with binary degrees of freedom, this can be achieved by choosing the initial state based on the Gray code [36], which ensures that the changes observed in the compression lengths are not stemming from discontinuities within the initial conditions [19]. For the compression algorithm, we use the `zlib.compress` function provided by Python 3.6.9., which provides a widely used implementation of [37], see appendix A for further details.

Generically, $\delta_n(t)$ will increase linearly with time in the long time limit. Therefore, the slope $S_\delta = \mathrm{d}\delta_n(t)/\mathrm{d}t$ of the characteristic exponent for sufficiently large n is the actual quantity that can be used to identify Class IV systems.

An additional complication may arise if different subsets of initial states give rise to different classes of dynamics. However, the classification presented in table 1 can still be applied. For example, if chaotic and unpredictable behavior are found among a subset of initial states, the overall slope S_δ will decrease due to the contribution of chaotic initial states, but the overall dynamics will still have a finite slope and hence classified as unpredictable.

Table 2. Ruleset for ECA rule $110 = 01101110_2$ indicating how the central site is updated. The ruleset for the corresponding rule 137 can be found by inverting all inputs and outputs.

State at t	111	110	101	100	011	010	001	000
Central site at $t+1$	0	1	1	0	1	1	1	0

3. Embedding of elementary CA

Elementary CA (ECAs) [38] are two-level systems on a 1D lattice, where the state i at the dimensionless time $t+1$ depends only on the states of the sites $i-1$, i, and $i+1$ and time t. In total, there are $2^{2^3} = 256$ different possible ECA rules, which can be enumerated according to the binary representation of their ruleset. Here, we will be interested in rule 110 (or its binary complement 137), see table 2 for the ruleset, as this ECA has been proven to be capable of universal computation [9] and hence belongs into Class IV.

Most ECA rules are irreversible, as each output bit depends on three input bits. This prevents an implementation in a quantum system in terms of unitary operations and instead requires the use of a dissipative quantum channel $\mathcal{V}$ providing the mapping $\rho(t+1) = \mathcal{V}\rho(t)$ for the quantum state ρ. The Liouvillian, which is the generator of such a quantum channel, can be expressed in terms of a purely dissipative quantum master equation in Lindblad form,

$$\frac{\mathrm{d}}{\mathrm{d}t}\rho = \gamma \sum_i \left(c_i \rho c_i^\dagger - \frac{1}{2}\left\{ c_i^\dagger c_i, \rho \right\} \right), \tag{2}$$

with c_i being the associated quantum jump operators [39] and γ being the characteristic rate of the dynamics. Note that the channel $\mathcal{V}$ is only implemented in the steady state, i.e. in the infinite time limit, see appendix B. For the case of a finite evolution time t_c, this means that the evolution of the corresponding cellular automaton becomes probabilistic. However, since a finite error rate can be recovered in classical systems by error correction codes, one can expect that Class IV systems capable of universal computation can tolerate a finite amount of computational errors introduced by the probabilistic update scheme. Interestingly, this setting allows to treat the cycle time t_c as a control parameter, which allows to alter the dynamical properties of the system under consideration in a relatively simple way.

For practical implementation purposes, it is highly desirable that the quantum jump operators are quasi-local, i.e. they act only on a small subset of the total Hilbert space. Within the ECA framework, this can be readily achieved by considering a second copy of the system, in which the state at time $t+1$ is prepared, see figure 1(a). After a time t_c, the role of the two copies is reversed and the second copy is taken as the input for the creation of the new state at time $t+2$ in the first copy. Note that these cyclic update scheme result in the Liouvillian being time-dependent and one cannot compute the complexity class by inspecting the spectrum of the Liouvillian.

4. Cycle time phase transition

4.1. Purely classical dynamics

Let us now turn to investigating how the dynamics of the rule 110 CA change with the cycle time t_c. Since the dynamics is purely classical, the master equation can be simulated efficiently using Monte-Carlo sampling. Figure 1(c) shows that the slope of the characteristic compression exponent S_δ indeed undergoes a phase transition from a chaotic Class III phase (figure 1(b)) with vanishing S_δ to an unpredictable Class IV phase (figure 1(d)) with finite S_δ. We also observe that the value of S_δ significantly depends on the system size N, which can be attributed to the appearance of emergent glider structures, i.e. sequences of triangular patterns, much larger than the three-site unit cell of the CA [9]. For example, the smallest system size in which all types of gliders can be realized is $N = 11$. Nevertheless, we can still perform finite size scaling of S_δ by considering only those system sizes at which S_δ is at a local maximum, a technique that has been used previously in the analysis of systems with strong incommensurability effects [40, 41]. Here, we find the phase transition to occur at $t_c = 5.80 \pm 0.08$ in the thermodynamic limit. Note that it might seem surprising that we are able to perform finite size scaling in a system with unpredictable behavior, as unpredictability is directly tied to a breakdown of finite size scaling theory [4]. This rules out to treat S_δ/N as an order parameter for unpredictability. However, here one of the two phases has the computable value of zero for S_δ

Table 3. Ruleset to prepare the Rokhsar–Kivelson state $|\psi_{RK}\rangle$. The operator $\mu_{\bar{i}} = P_{\bar{i}-1}|-\rangle\langle+|_{\bar{i}}P_{\bar{i}+1}$ acts on the three sites surrounding $\bar{i}$ on the output ring, with $|\pm\rangle = (|0\rangle \pm |1\rangle)$. The operator σ_- acts only on the site $\bar{i}$.

State k at t	111	110	101	100	011	010	001	000
Operation O_k	μ	σ_-	μ	μ	μ	μ	μ	μ

in the thermodynamic limit, which means that the phase transition can successfully detected by observing deviations from S_δ vanishing for increasing system sizes.

4.2. Competition with entanglement

So far, we have not addressed including quantum fluctuations into the dynamics. While there are many different proposals for CA dynamics within quantum systems [11, 14, 16, 17, 42–44], here we focus on the case where we have two competing dynamics $\mathcal{L}_c$ and $\mathcal{L}_q$, which are both generators satisfying the purely dissipative Lindblad form of equation (2), i.e. the full Lindblad generator $\mathcal{L}$ is given by

$$\mathcal{L} = \sin^2\left(\phi\frac{\pi}{2}\right)\mathcal{L}_c + \cos^2\left(\phi\frac{\pi}{2}\right)\mathcal{L}_q, \tag{3}$$

where ϕ is a parameter that interpolates between the fully quantum and fully classical dynamics. This approach has the advantage that the relevant observable S_δ for detecting unpredictability can be carried over to the quantum case by identifying the ith bit in the string S_j by the most likely measurement result when sampled over many trajectories.

In the following, we will be interested in the case where the quantum part of the dynamics is carefully chosen to have its unique steady state being highly entangled. For this, we choose a recently introduced quantum master equation that prepares the system in a Rokhsar–Kivelson state [20], which is given by

$$|\psi_{RK}\rangle = \frac{1}{\sqrt{Z}}\prod_k^N (1 - P_{k-1}\sigma_+^k P_{k+1})|00\cdots0\rangle, \tag{4}$$

where $P_k = |0\rangle\langle0|_k$, $\sigma_+^k = |1\rangle\langle0|_k$, and Z is a normalization constant. This state is an equal-weight superposition of all states that have no adjacent qubits in the $|1\rangle$ state. To give an example, the RK state for $N = 4$ is equal to

$$|\psi_{RK}\rangle_4 = \frac{1}{\sqrt{7}}\Big(|0000\rangle - |1000\rangle - |0100\rangle - |0010\rangle - |0001\rangle + |1010\rangle + |0101\rangle\Big). \tag{5}$$

The jump operators c_i^q required to prepare $|\psi_{RK}\rangle$ can be brought into a similar form as the one for the rule 110, i.e.

$$c_i^q = \sum_k O_{\bar{i},k}Q_{i,k}, \tag{6}$$

where $O_{\bar{i},k}$ is an operator acting on the sites $i-1$, i, and $i+1$ on the *output* ring, while $Q_{i,k} = |k\rangle\langle k|$ is a three-body projection operator acting on the corresponding sites of the *input* ring. The index k runs over all eight basis states on the sites $i-1$, i, and $i+1$. Table 3 shows a set of operators that lead to $|\psi_{RK}\rangle$ being the dark state of the dynamics, satisfying $c_i^q|\psi_{RK}\rangle = 0$. Importantly, since $[O_{i,k}, O_{i\pm1,k}] \neq 0$ for $k \neq 110$, $\mathcal{L}_q$ is capable of generating entanglement even in the absence of any Hamiltonian dynamics.

To observe the interplay between unpredictability and entanglement, it is helpful to make the two competing dynamics more compatible with each other. Increasing the compatibility is desirable as the generation of superposition states necessary to observe entanglement is adding quantum fluctuations to the unpredictability measure, see appendix B for details. In particular, one can see that $|\psi_{RK}\rangle$ will have more 0 s than 1 s in its binary representation due to the action of the projection operators P_k. On the other hand, the dynamics of rule 110 is slightly biased towards the 1 state, as there are more 1 s than 0 s in the output set. Therefore, we consider the binary complement rule $137 = 10001001_2$, which is then also biased towards the 0 state, but having otherwise identical properties as rule 110.

To further align the two competing dynamics, we additionally split the dynamics into two parts, each being $t_c/2$ long. During the first part, both the classical part $\mathcal{L}_c$ and the quantum part $\mathcal{L}_q$ are active, while during the second part only the classical dynamics is acting on the system. Importantly, the second part recovers the classical patterns which are affected by quantum fluctuations in the first half of the cycle time provided that t_c is sufficiently large. In this setting, all observables are evaluated at the time $t_c/2$.

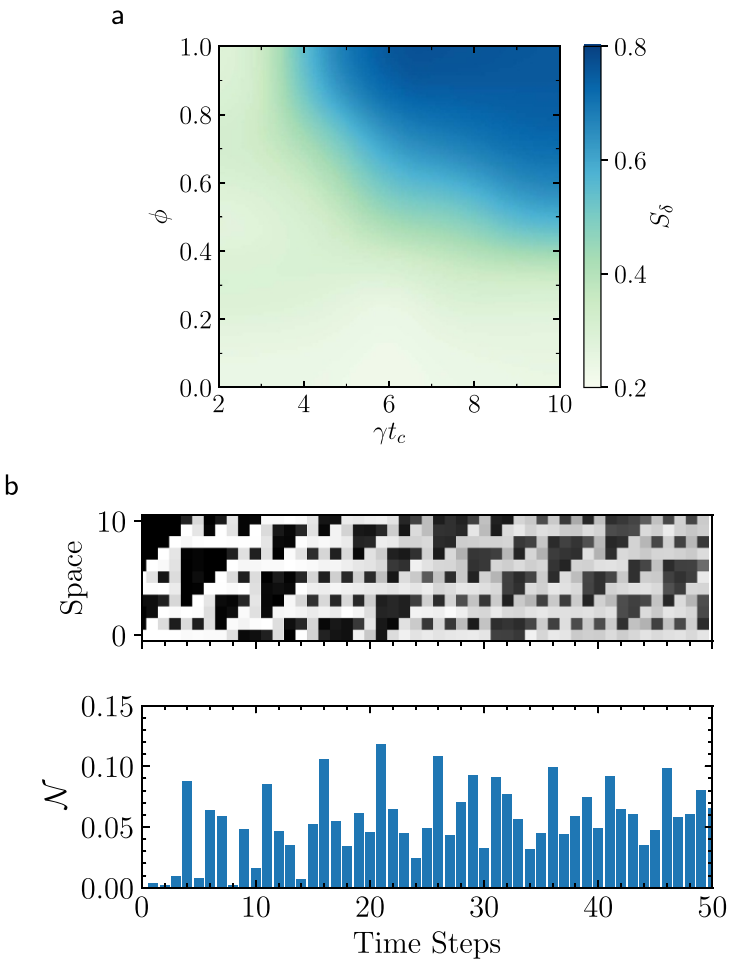

Figure 2. Competition between classical and quantum dynamics. (a) Slope S_δ of the characteristic compression exponent as a function of the cycle time t_c and the interpolation parameter ϕ, showing an extended region of unpredictable Class IV behavior even in the presence of quantum fluctuations. (b) Average over 50 Monte-Carlo samples of a single initial configuration for $\gamma t_c = 10$ and $\phi = 0.6$. Although quantum fluctuations lead to a washing out of the patterns, the emergent structures remain clearly visible. The negativity $\mathcal{N}$ (between even and odd sites) rapidly increases and remains finite in the long time limit (The time steps are of length $\gamma t_c = 10$ and they correspond to the midpoint of each cycle time). In other words, entanglement persists also for values of ϕ that lead to unpredictable dynamics, i.e. entanglement and unpredictability are not mutually exclusive.

Let us now turn to a numerical investigation of the competition between the classical rule 137 dynamics $\mathcal{L}_c$ and the quantum dynamics $\mathcal{L}_q$ preparing the Rokhsar–Kivelson state. Figure 2 shows the unpredictability of the system in terms of the slope S_δ of the characteristic compression exponent as a function of the cycle time t_c and the interpolation parameter ϕ, as well as the entanglement of the system in terms of the negativity

$$\mathcal{N}(\rho) = \frac{\left\|\rho^{T_A}\right\|_1 - 1}{2}, \tag{7}$$

where $\|.\|_1$ denotes the trace norm and ρ^{T_A} is the partial transpose of ρ with respect to the subsystem A [45]. In this case, we consider all odd sites as the subsystem A to be able to compute entanglement spreading over the entire output ring. Calculations were performed using massively parallelized wave-function Monte-Carlo simulations [46] for 22 sites (see appendix C), improving the previously reported largest system size for simulations retaining the full Hilbert space [47]. This allows us to study unpredictability as 11 sites on each ring is the smallest system size potentially supporting class IV behavior. For the classical limit $\phi \to 1$, we recover the classical transition to an unpredictable Class IV phase reported in section 4.1. However, this transition remains observable away from the classical limit as well. Crucially, we also find a nonzero negativity for sufficiently low values of ϕ, meaning that unpredictability and entanglement can coexist in the system. Finally, when the interpolation parameter ϕ is decreased further, unpredictable Class IV behavior is destroyed by quantum fluctuations. Interestingly, our results suggest that Class IV behavior can be broken up into distinct sub-classes, at least in the quantum case. Here, we observe two possible types of dynamics, depending on whether the system is asymptotically entangled or not.

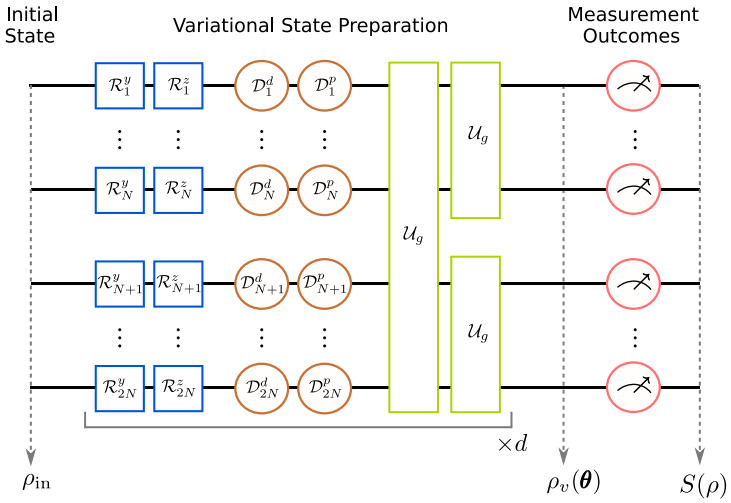

Figure 3. Sketch of the variational quantum simulation scheme. A quantum state $\rho_v(\boldsymbol{\theta})$ is generated from an initial state $\rho_{\rm in}$ and a set of variational parameters $\boldsymbol{\theta} = \{\boldsymbol{\theta}_n\}_{n=1}^{d}$ for d layers. The variational circuit consists of local Pauli rotations $\mathcal{R}(\boldsymbol{\theta}_n)$, local dissipation operators $\mathcal{D}(\boldsymbol{\theta}_n)$, and global unitary operations $\mathcal{U}_g(\boldsymbol{\theta}_n)$.

5. Variational quantum simulation (VQS)

The realization of the jump operators for the classical and quantum dynamics requires the implementation of four and six-body interactions, respectively. While such high-order interactions can be readily engineered in digital quantum simulators [48, 49], recently developed techniques for the variational preparation of quantum states [23–25] can be adapted for the quantum simulation of open system dynamics, especially on noisy intermediate-scale quantum devices. Basically, VQS is a hybrid classical-quantum approach that can approximately reproduce the dynamics of a quantum system without explicit realization of the corresponding Hamiltonian.

Within our VQS approach, we can realize the time evolution of largely arbitrary open quantum many-body systems according to a Lindblad quantum master equation. To this end, we consider the dynamics of an observable O in the Heisenberg picture,

$$\frac{\mathrm{d}O}{\mathrm{d}t} \equiv \mathcal{L}_H O = i[H,O] + \sum_i^N L_i^\dagger O L_i - \frac{1}{2}\{L_i^\dagger L_i, O\}. \tag{8}$$

The strategy behind VQS is to consider a variational parametrization of the state $\rho(t+\tau)$ after a continuous timestep τ, given the state $\rho(t)$ at time t and the dynamics according to the quantum master equation. Our approach is based on the variational principle for open quantum systems [50], which also has been generalized towards variational approximation of the time evolution, both in the Schrödinger [51] and in the Heisenberg picture [52]. Within the latter, one can introduce a variational cost functional F_v given by

$$F_v = \sum_i \left| \langle O_i(t+\tau)\rangle - \langle O_i(t)\rangle - \frac{\tau}{2}\mathcal{L}_H[O_i(t) + O_i(t+\tau)] \right|, \tag{9}$$

which realizes a discretized version of the master equation that is correct up to second order in τ. Crucially, the sum does not need to run over a complete set of observables to achieve accurate results [52].

Having defined the variational cost function, we also need to specify the parameterization of the density matrix ρ using a set of variational parameters $\boldsymbol{\theta}$. For this, we consider a variational circuit consisting of three parts, see figure 3: (i) coherent single qubit rotations, (ii) dissipative single qubit damping, and (iii) global unitary time evolution under an interacting many-body Hamiltonian that can be implemented efficiently.

To be specific, we envision the qubits stored in the hyperfine ground states of ultracold atoms trapped in an optical tweezer array [53, 54]. While the coherent single qubit rotations are following from standard Pauli rotations around two independent axes using microwave driving, the dissipative dynamics is governed by two separate quantum channels realized by dissipative optical pumping of the qubit states ($\mathcal{D}_d$) and phase fluctuations mediated by noisy laser driving ($\mathcal{D}_p$), respectively. In the operator sum representation [55] the two channels can be written as

$$\mathcal{D}_\mu(\rho) = \frac{1}{N}\sum_{j=1}^{N}\left[D_{\mu_1}^{(j)}\rho D_{\mu_1}^{(j)\dagger} + D_{\mu_2}^{(j)}\rho D_{\mu_2}^{(j)\dagger}\right], \tag{10}$$

where $\mu \in \{d, p\}$ and

$$D_{d_1} = \sqrt{1-e^{-\theta_d}}\sigma_-, \tag{11}$$

$$D_{d_2} = P_0 + e^{-\theta_d/2}P_1, \tag{12}$$

$$D_{p_1,p_2} = \sqrt{\frac{e^{-\theta_p/2}}{2}} \pm \sqrt{\frac{(1-e^{-\theta_p})}{2}}\sigma_z, \tag{13}$$

depending on the variational parameters θ_d and θ_p. Finally, the global unitaries $\mathcal{U}_g$ are implemented based on coupling the $|1\rangle$ state to a strongly interacting Rydberg state in a Rydberg dressing configuration [56–59], giving rise to the effective Hamiltonian

$$H_0 = \frac{\Omega}{2}\sum_i \sigma_x^{(i)} + \sum_{i<j}\frac{C_6}{|\mathbf{r}_i - \mathbf{r}_j|^6}P_1^{(i)}P_1^{(j)}, \tag{14}$$

where Ω indicates the Rabi frequency of the driving field and C_6 denotes the effective van der Waals coefficient of the Rydberg-dressed state. The global unitaries act first on both of the rails at the same time and then subsequently on each rail independently. The times t_1 and t_2 of these steps provide two additional variational parameters.

Let us now benchmark our VQS procedure for the quantum rule 137 dynamics using two rings of $N = 3$ sites. In our simulations, we set $C_6/\Omega = 100$ as this corresponds to a Rydberg blockade radius $r_b = \sqrt{6}C_6/\Omega \approx 2.15$ in units of the lattice spacing, which is comparable to the range of the multi-qubit jump operators in the quantum master equation. Furthermore, we choose a variational circuit depth of $d = 3$. For the set of observables entering the variational cost function (9), we choose a complete set of three-local Pauli operators per site, i.e. $4^3 = 64$ observables. Numerical optimization of the highly non-linear cost function is performed using a sequential quadratic programming algorithm [60] in a layerwise fashion to avoid getting stuck in barren plateaus [61].

Figure 4(a) shows variational norm F_v and error probability ε between the exact density matrix ρ and variational state $\rho_v(\boldsymbol{\theta})$ at time t, defined in terms of the fidelity F as

$$\varepsilon = 1 - F = 1 - \left[\mathrm{Tr}\sqrt{\sqrt{\rho_v(\boldsymbol{\theta})}\rho\sqrt{\rho_v(\boldsymbol{\theta})}}\right]^2. \tag{15}$$

For $\phi = 0.5$ and $\gamma t_c = 10$, where unpredictability and quantum entanglement coexist, the results indicate overall errors less than 2% for almost all data points. Figure 4(b) demonstrates that entanglement measured in terms of the negativity also shows good quantitative agreement with the exact dynamics, underlining the power of the VQS approach.

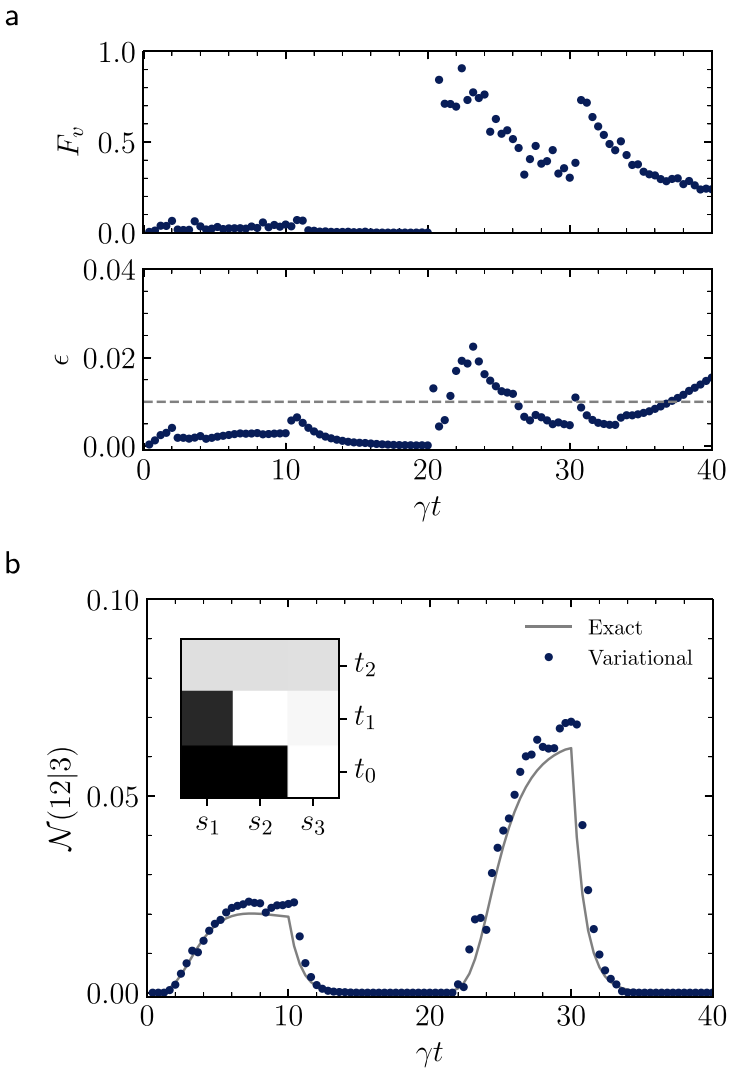

Figure 4. Benchmarking of the VQS approach for $\phi = 0.5$ and $\gamma t_c = 10$ for a system of $N = 3$ sites, using $d = 3$ variational layers. Variational norm F_v, error probability ε (a) and quantum negativity $\mathcal{N}$ (b) as a function of time for the first two timesteps. The inset shows the density pattern in the output ring at the middle of the steps.

6. Conclusion

In summary, our work establishes a novel dynamical class of open quantum many-body systems that allow to study the interplay between computational properties and quantum effects. Strikingly, we have shown that computational unpredictability is not incompatible with quantum entanglement, but that the two can coexist with each other for a long time. Given the inherent difficulty to simulate open quantum systems on classical computers [62], these systems are also excellent candidates to observe a quantum advantage. Our results on the VQS suggest that the interplay between entanglement and unpredictability can be experimentally realized using present technologies. In the future, it will be also interesting to develop quantum analogs of the data compression approach for Class IV systems, using quantum compression algorithms [63–66].

Data availability statement

All data that support the findings of this study are included within the article (and any supplementary files).

Acknowledgments

The authors acknowledge fruitful discussion with R van Bijnen on variational quantum simulation. This work was funded by the Volkswagen Foundation, by the Deutsche Forschungsgemeinschaft (DFG, German Research Foundation) within SFB 1227 (DQ-mat, project A04), SPP 1929 (GiRyd), and under Germanys Excellence Strategy—EXC-2123 QuantumFrontiers - 390837967.

Table 4. Gray code enumeration of initial states. Each state only has a single bit differing with its adjacent state, i.e. the Hamming distance between two adjacent states is 1. Here, the first 12 states of the Gray code are shown.

Gray-code pure state j	
$\|\psi_0\rangle = \|00\ldots00000\rangle$	$\|\psi_6\rangle = \|00\ldots01111\rangle$
$\|\psi_1\rangle = \|00\ldots00001\rangle$	$\|\psi_7\rangle = \|00\ldots01011\rangle$
$\|\psi_2\rangle = \|00\ldots00011\rangle$	$\|\psi_8\rangle = \|00\ldots01001\rangle$
$\|\psi_3\rangle = \|00\ldots00111\rangle$	$\|\psi_9\rangle = \|00\ldots11001\rangle$
$\|\psi_4\rangle = \|00\ldots00101\rangle$	$\|\psi_{10}\rangle = \|00\ldots11011\rangle$
$\|\psi_5\rangle = \|00\ldots01101\rangle$	$\|\psi_{11}\rangle = \|00\ldots11111\rangle$

Appendix A. Compressed length of mixed states

In this appendix, we explain the procedure required to compute the characteristic compression exponent given the mixed-state representation of the two-ring ECA dynamics. We first initialize the input ring as well as the output ring as

$$\rho_j(t=0) = |\psi_j\rangle\langle\psi_j|_{\text{output}} \otimes |\psi_j\rangle\langle\psi_j|_{\text{input}}, \tag{A1}$$

where $|\psi_j\rangle$ denotes the jth Gray-code state, see table 4. We only consider $j \geqslant 1$, as the system needs at least one excitation to initiate a non-trivial dynamics.

Next, we need to obtain a string representation of a given mixed state on the output ring. For this, we employ a repeated random sampling based on the Monte-Carlo method. Following that, we introduce a digitized version $\Pi_{i,j}(t) = [P^{\text{traj}}_{i,j}(t)]$ of a single-trajectory occupation probability $P^{\text{traj}}_{i,j}(t)$ of the site i at time t for the jth initial state, with $[\cdot]$ being the rounding operation. The Monte-Carlo approach is advantageous specifically for the classical case where the rounding is exact, i.e. $P^{\text{traj}}_{i,j}(t) \in \{0,1\}$. A single-trajectory string representation is then constructed as

$$\begin{aligned} S^{\text{traj}}_j(t) = {} & \Pi_{1,j}(0) \oplus \Pi_{2,j}(0) \oplus \ldots \oplus \Pi_{N,j}(0) \\ & \oplus \Pi_{1,j}(1) \oplus \Pi_{2,j}(1) \oplus \ldots \oplus \Pi_{N,j}(1) \oplus \ldots \oplus \Pi_{1,j}(t) \oplus \Pi_{2,j}(t) \oplus \ldots \oplus \Pi_{N,j}(t), \end{aligned} \tag{A2}$$

indicates a sample of all the N sites on the output ring evolving from an initial state $\rho_j(t_0)$ until an arbitrary (discrete) time t, i.e. a string consists of $N(t+1)$ bits. Here, $\oplus$ refers to concatenation of the binary digits.

Having computed a binary string S, we employ a lossless data-compression algorithm to compute the compressed length $\mathcal{C}_c(S)$. To this end, we use a Python implementation of the DEFLATE algorithm provided by the `zlib` module in Python 3.6.9. The `compress` function in this module returns a compressed representation of the given data in bytes. The desired compressed length is then computed by

$$\mathcal{C}_c(S) = \texttt{len}\left(\texttt{zlib.compress}(S)\right), \tag{A3}$$

where `len` returns the string length of the compressed data. Importantly, the compressed length should reflect genuine properties of the given string regardless of the choice of the compression algorithm. We have validate this numerically for different lossless algorithms. However, there might be minor quantitative differences for different algorithms which originates from the fact that optimal data compression is also undecidable.

Now, we are in the position to calculate the characteristic compression exponent using the resulting discretized data. To compute the averaged compressed length in equation (1) we incorporate sampled binary strings as follows

$$\bar{\mathcal{C}}_c(S_j(t)) = \sum_{\text{traj}=1}^{N_{\text{traj}}} \frac{\mathcal{C}_c(S^{\text{traj}}_j(t))}{N_{\text{traj}}}, \tag{A4}$$

where traj runs over N_{traj} samples. Hence, we perform a trajectory average over 50 trajectories for each initial state j. In practice, we observe good convergence of the results for $n = 40$ distinct initial states and final times of $t = 200$. We should emphasize that since the strings $S^{\text{traj}}_j(t)$ correspond to individual trajectories of the Monte-Carlo simulation, any function of the strings is also probabilistic as an artefact of the method's stochasticity. However, the measurement outcomes of the two-ring ECA are intrinsically probabilistic as they exhibit random fluctuations, both stemming from quantum fluctuations in the case of quantum dynamics and the probabilistic implementation of the ECA rules in the presence of a finite cycle time t_c.

Appendix B. Lindblad generator of elementary cellular automata

The quantization of ECA rules on the two-ring setup shown in figure 1 is based on the mapping

$$\rho(t+1) = e^{\mathbb{L}}\rho(t), \tag{B1}$$

where t denotes discrete time and $\mathbb{L}$ is the matrix form of the Lindblad generator

$$\mathcal{L} = \sin^2\left(\phi\frac{\pi}{2}\right)\mathcal{L}_c + \cos^2\left(\phi\frac{\pi}{2}\right)\mathcal{L}_q, \tag{B2}$$

which is composed of two Lindblad operators $\mathcal{L}_c$ and $\mathcal{L}_q$ defined in continuous time τ as

$$\mathcal{L}_{c/q}(\rho) = \gamma_{c/q}(\tau)\sum_i\left(c^i_{c/q}\rho {c^i_{c/q}}^\dagger - \frac{1}{2}\left\{{c^i_{c/q}}^\dagger c^i_{c/q}, \rho\right\}\right), \tag{B3}$$

with time-dependent dissipation rates $\gamma_c(\tau) = \gamma$ for the full cycle time t_c and $\gamma_q(\tau) = \gamma$ for $t \leqslant t_c/2$. The jump operators of the classical part are defined based on the corresponding ECA rule such that

$$c^c_i = \sigma^{\bar{i}}_-\sum_{k\in\mathcal{A}} Q_{i,k} + \sigma^{\bar{i}}_+\sum_{k\in\mathcal{B}} Q_{i,k}, \tag{B4}$$

where $\sigma^{\bar{i}}_- = |0\rangle\langle 1|_{\bar{i}}$ and $\sigma^{\bar{i}}_+ = |1\rangle\langle 0|_{\bar{i}}$ are lowering and raising operators respectively. $\bar{i}$ refers to site i on the output ring and k denotes a three-body state whose projection operator $Q_{i,k} = |k\rangle\langle k|$ acts on sites $i-1$, i, and $i+1$. Here, k runs over two subsets $\mathcal{A}$ and $\mathcal{B}$, which for the ECA rule 110 are given by

$$\begin{aligned}\mathcal{A} &= \{000, 100, 111\},\\ \mathcal{B} &= \{001, 010, 011, 101, 110\}.\end{aligned} \tag{B5}$$

To be explicit, the first summation in equation (B4) reads as

$$\sum_{k\in\mathcal{A}} Q_{i,k} = |000\rangle\langle 000|_{i-1,i,i+1} + |100\rangle\langle 100|_{i-1,i,i+1} + |111\rangle\langle 111|_{i-1,i,i+1}, \tag{B6}$$

and the second summation is the complement acting on the rest of the basis states, i.e.

$$\sum_{k\in\mathcal{B}} Q_{i,k} = I - \sum_{k\in\mathcal{A}} Q_{i,k}. \tag{B7}$$

In a similar fashion for the ECA rule 137 we have

$$\begin{aligned}\mathcal{A} &= \{001, 010, 100, 101, 110\},\\ \mathcal{B} &= \{000, 011, 111\}.\end{aligned} \tag{B8}$$

Additionally, we define the jump operators of the quantum part as

$$c^q_i = \sigma^{\bar{i}}_-|110\rangle\langle 110|_{i-1,i,i+1} + P_{\bar{i}-1}|-\rangle\langle +|_{\bar{i}}P_{\bar{i}+1}\sum_{k\neq 110} Q_{i,k}, \tag{B9}$$

where the first term removes trivial steady states by populating the 0 state on the output ring and the second term generates entangled states by a three-body operation on the output ring provided that the corresponding the-body state k on the input ring is not equal to 110.

Appendix C. Monte-Carlo sampling of unpredictable dynamics

We here outline the main steps of the wave-function Monte-Carlo method that we utilized in our numerical simulation. The advantage of this method comes from the fact that a density matrix is essentially a statistical ensemble of pure states. This allows breaking the quadratic complexity of a density matrix by decomposing it into (several) wave functions as their complexity is linear in terms of the Hilbert space dimension. Therefore, instead of evolving the whole density matrix through time, one can evolve individual pure states to a desired time and then compute the expectation values of the observable of interest according to standard Monte-Carlo sampling. To be explicit, each trajectory is evolved according to an effective non-Hermitian Hamiltonian $H_{\text{eff}} = H - \frac{i}{2}\sum_i c_i^\dagger c_j$ describing the dissipative dynamics of the underlying open system. In our

model, the Liouvillian is purely dissipative, i.e. $H = 0$ and we define the total set of jump operators as following

$$c = \left\{ \left[\sin^2 \left(\phi \frac{\pi}{2} \right) \gamma_c(t) \right]^{1/2} c_c^i, \left[\cos^2 \left(\phi \frac{\pi}{2} \right) \gamma_q(t) \right]^{1/2} c_q^i \right\}_{i=1}^{N}, \tag{C1}$$

which means that in total there are $2N$ jump operators. Now, to implement the trajectory propagation using the effective Hamiltonian of our system, one can follow the steps below:

1. Pick an initial pure state $|\psi(t_0)\rangle = |\psi_j\rangle_{\text{output}} \otimes |\psi_j\rangle_{\text{input}}$ given the Gray-code state j;
2. Choose a random number $r = [0, 1]$ standing for the occurrence of a quantum jump;
3. Evolve the state using the effective Hamiltonian $|\psi(t)\rangle = \exp(-iH_{\text{eff}}t)|\psi(t_0)\rangle$ up to the time t_k where $\langle\psi(t_k)|\psi(t_k)\rangle = r$. Here, t_k denotes the time that a specific jump occurs, say c_n in which n determines the site index i plus the type of the jump, i.e. c or q;
4. Determine n such that $P_n \geqslant r$ with $P_n = \sum_{i=1}^{n} \langle\psi(t_k)|c_i^\dagger c_i|\psi(t_k)\rangle / \delta p$ where δp normalizes the probability P_n;
5. Calculate the after-jump state $|\psi(t_k)\rangle' = c_n|\psi(t_k)\rangle / \langle\psi(t_k)|c_n^\dagger c_n|\psi(t_k)\rangle^{1/2}$;
6. If the time t corresponds to the middle of a cycle time, calculate compressed length of the single-trajectory binary representation with respect to the output ring $\mathcal{C}_c(S_j^{\text{traj}}(t))$;
7. If the time t corresponds to the end of a cycle time, switch the rings by converting $c_i \leftrightarrow c_{\bar{i}}$;
8. Replace $|\psi(t_0)\rangle$ with the new state and repeat the steps.

The algorithm above outputs the time evolution of a single trajectory for a given initial state. This treatment makes it possible to speed up the simulation by running the computations with respect to different trajectories in parallel.

ORCID iD

Javad Kazemi https://orcid.org/0000-0002-3176-8077

References

[1] Gödel K 1931 Über formal unentscheidbare Sätze der principia mathematica und verwandter systeme I *Monatsh. Math. Phys.* **38** 173
[2] Turing A M 1937 On computable numbers, with an application to the entscheidungsproblem *Proc. London Math. Soc.* **s2-42** 230
[3] Lloyd S 1993 Quantum-mechanical computers and uncomputability *Phys. Rev. Lett.* **71** 943
[4] Cubitt T S, Perez-Garcia D and Wolf M M 2015 Undecidability of the spectral gap *Nature* **528** 207
[5] Shiraishi N and Matsumoto K 2021 Undecidability in quantum thermalization *Nat. Commun.* **12** 5084
[6] Wolfram S 1984 Universality and complexity in cellular automata *Physica* D **10** 1
[7] Margolus N 1984 Physics-like models of computation *Physica* D **10** 81
[8] Berlekamp E, Conway J and Guy R 2004 *Winning Ways for Your Mathematical Plays* vol 4 (A K Peters)
[9] Cook M 2004 Universality in elementary cellular automata *Complex Syst.* **15** 1
[10] Neary T and Woods D 2006 P-completeness of cellular automaton rule 110 *Automata, Languages and Programming: 33rd Int. Colloquium, ICALP 2006* (*Lecture Notes in Computer Science* vol 4051) vol **4051** p 132
[11] Brennen G K and Williams J E 2003 Entanglement dynamics in one-dimensional quantum cellular automata *Phys. Rev.* A **68** 042311
[12] Raussendorf R 2005 Quantum cellular automaton for universal quantum computation *Phys. Rev.* A **72** 022301
[13] Arrighi P, Nesme V and Werner R 2008 *Language and Automata Theory and Applications* ed C Martín-Vide, F Otto and H Fernau (Springer) pp 64–75
[14] Bleh D, Calarco T and Montangero S 2012 Quantum game of life *Europhys. Lett.* **97** 20012
[15] Hillberry L E, Jones M T, Vargas D L, Rall P, Halpern N Y, Bao N, Notarnicola S, Montangero S and Carr L D 2021 Entangled quantum cellular automata, physical complexity and goldilocks rules *Quantum Sci. Technol.* **6** 045017
[16] Lesanovsky I, Macieszczak K and Garrahan J P 2019 Non-equilibrium absorbing state phase transitions in discrete-time quantum cellular automaton dynamics on spin lattices *Quantum Sci. Technol.* **4** 02LT02
[17] Wintermantel T M, Wang Y, Lochead G, Shevate S, Brennen G K and Whitlock S 2020 Unitary and nonunitary quantum cellular automata with Rydberg arrays *Phys. Rev. Lett.* **124** 070503
[18] Wolfram S 1983 Statistical mechanics of cellular automata *Rev. Mod. Phys.* **55** 601
[19] Zenil H 2010 Compression-based investigation of the dynamical properties of cellular automata and other systems *Complex Syst.* **19** 1
[20] Roghani M and Weimer H 2018 Dissipative preparation of entangled many-body states with Rydberg atoms *Quantum Sci. Technol.* **3** 035002
[21] Browaeys A and Lahaye T 2019 Many-body physics with individually controlled Rydberg atoms *Nat. Phys.* **16** 132
[22] Morgado M and Whitlock S 2021 Quantum simulation and computing with Rydberg-interacting qubits *AVS Quantum Sci.* **3** 023501
[23] Peruzzo A, McClean J, Shadbolt P, Yung M-H, Zhou X-Q, Love P J, Aspuru-Guzik A and O'Brien J L 2014 A variational eigenvalue solver on a photonic quantum processor *Nat. Commun.* **5** 4213
[24] Moll N *et al* 2018 Quantum optimization using variational algorithms on near-term quantum devices *Quantum Sci. Technol.* **3** 030503

[25] Kokail C *et al* 2019 Self-verifying variational quantum simulation of lattice models *Nature* **569** 355
[26] Martinez G J, Seck-Tuoh-Mora J C and Zenil H 2013 Computation and universality: class IV versus class III cellular automata *J. Cell. Autom.* **7** 393
[27] Sacha K and Zakrzewski J 2017 Time crystals: a review *Rep. Prog. Phys.* **81** 016401
[28] Eckmann J P and Ruelle D 1985 Ergodic theory of chaos and strange attractors *Rev. Mod. Phys.* **57** 617
[29] Tél T and Gruiz M 2006 *Chaotic Dynamics: an Introduction Based on Classical Mechanics* (Cambridge University Press)
[30] Langton C G 1990 Computation at the edge of chaos: phase transitions and emergent computation *Physica* D **42** 12
[31] Adamatzky A 2010 *Game of Life Cellular Automata* vol 1 (Springer)
[32] Cotler J, Hunter-Jones N, Liu J and Yoshida B 2017 Chaos, complexity and random matrices *J. High Energy Phys.* **2017** 48
[33] Koppel M 1987 Complexity, depth and sophistication *Complex Syst.* **1** 1087
[34] Aaronson S, Carroll S M and Ouellette L 2014 Quantifying the rise and fall of complexity in closed systems: the coffee automaton, (arXiv:1405.6903)
[35] Li M and Vitányi P 2008 *An Introduction to Kolmogorov Complexity and Its Applications* (*Texts in Computer Science*) (Springer)
[36] Gray F 1953 Pulse code communication *US Patent No.* 2,632,058
[37] Deutsch L P 1996 *DEFLATE Compressed Data Format Specification Version 1.3, RFC 1951* (RFC Editor)
[38] Wolfram S 1984 Cellular automata as models of complexity *Nature* **311** 419
[39] Breuer H-P and Petruccione F 2002 *The Theory of Open Quantum Systems* (Oxford University Press)
[40] Weimer H and Büchler H P 2010 Two-stage melting in systems of strongly interacting Rydberg atoms *Phys. Rev. Lett.* **105** 230403
[41] Arora A, Morse D C, Bates F S and Dorfman K D 2015 Commensurability and finite size effects in lattice simulations of diblock copolymers *Soft Matter* **11** 4862
[42] Arrighi P 2019 An overview of quantum cellular automata *Nat. Comput.* **18** 885
[43] Farrelly T 2020 A review of quantum cellular automata *Quantum* **4** 368
[44] Klobas K, Bertini B and Piroli L 2021 Exact thermalization dynamics in the rule 54 quantum cellular automaton *Phys. Rev. Lett.* **126** 160602
[45] Vidal G and Werner R F 2002 Computable measure of entanglement *Phys. Rev.* A **65** 032314
[46] Johansson J, Nation P and Nori F 2013 QuTiP 2: a Python framework for the dynamics of open quantum systems *Comp. Phys. Comm.* **184** 1234
[47] Raghunandan M, Wrachtrup J and Weimer H 2018 High-density quantum sensing with dissipative first order transitions *Phys. Rev. Lett.* **120** 150501
[48] Weimer H, Müller M, Lesanovsky I, Zoller P and Büchler H P 2010 A Rydberg quantum simulator *Nat. Phys.* **6** 382
[49] Weimer H, Müller M, Büchler H P and Lesanovsky I 2011 Digital quantum simulation with Rydberg atoms *Quantum Inf. Proc.* **10** 885
[50] Weimer H 2015 Variational principle for steady states of dissipative quantum many-body systems *Phys. Rev. Lett.* **114** 040402
[51] Overbeck V R and Weimer H 2016 Time evolution of open quantum many-body systems *Phys. Rev.* A **93** 012106
[52] Pistorius T and Weimer H 2021 Variational analysis of driven-dissipative bosonic fields *Phys. Rev.* A **104** 063711
[53] Endres M, Bernien H, Keesling A, Levine H, Anschuetz E R, Krajenbrink A, Senko C, Vuletic V, Greiner M and Lukin M D 2016 Atom-by-atom assembly of defect-free one-dimensional cold atom arrays *Science* **354** 1024
[54] Barredo D, de Léséleuc S, Lienhard V, Lahaye T and Browaeys A 2016 An atom-by-atom assembler of defect-free arbitrary two-dimensional atomic arrays *Science* **354** 1021
[55] Nielsen M A and Chuang I L 2000 *Quantum Computation and Quantum Information* (Cambridge University Press)
[56] Glaetzle A W, Dalmonte M, Nath R, Gross C, Bloch I and Zoller P 2015 Designing frustrated quantum magnets with laser-dressed Rydberg atoms *Phys. Rev. Lett.* **114** 173002
[57] Zeiher J, van Bijnen R, Schauß P, Hild S, Choi J-Y, Pohl T, Bloch I and Gross C 2016 Many-body interferometry of a Rydberg-dressed spin lattice *Nat. Phys.* **12** 1095
[58] Overbeck V R, Maghrebi M F, Gorshkov A V and Weimer H 2017 Multicritical behavior in dissipative Ising models *Phys. Rev.* A **95** 042133
[59] Helmrich S, Arias A and Whitlock S 2018 Uncovering the nonequilibrium phase structure of an open quantum spin system *Phys. Rev.* A **98** 022109
[60] Virtanen P *et al* 2020 SciPy 1.0: fundamental algorithms for scientific computing in Python *Nat. Methods* **17** 261
[61] McClean J R, Boixo S, Smelyanskiy V N, Babbush R and Neven H 2018 Barren plateaus in quantum neural network training landscapes *Nat. Commun.* **9** 4812
[62] Weimer H, Kshetrimayum A and Orús R 2021 Simulation methods for open quantum many-body systems *Rev. Mod. Phys.* **93** 015008
[63] Schumacher B 1995 Quantum coding *Phys. Rev.* A **51** 2738
[64] Jozsa R, Horodecki M, Horodecki P and Horodecki R 1998 universal quantum information compression *Phys. Rev. Lett.* **81** 1714
[65] Rozema L A, Mahler D H, Hayat A, Turner P S and Steinberg A M 2014 Quantum data compression of a qubit ensemble *Phys. Rev. Lett.* **113** 160504
[66] Romero J, Olson J P and Aspuru-Guzik A 2017 Quantum autoencoders for efficient compression of quantum data *Quantum Sci. Technol.* **2** 045001